A predictive formula for the electron stopping power

A. Jablonski[a], S. Tanuma[b] and C. J. Powell[c]
[a]*Institute of Physical Chemistry, Polish Academy of Sciences, ul. Kasprzaka 44/52, 01-224 Warsaw, Poland*
[b]*Materials Analysis Station, National Institute for Materials Science, 1-2-1 Sengen, Tsukuba, Ibaraki 305-0047, Japan*
[c]*Surface and Microanalysis Science Division, National Institute of Standards and Technology, Gaithersburg, Maryland 20899-8370, USA*

(Received: January 31, 2006 ; Accepted: April 20, 2006)

We describe a new analytical formula for the electron stopping power (SP) that was developed for electron energies between 200 eV and 30 keV. This formula describes the product of the SP and the inelastic mean free path (IMFP), and is a simple function of atomic number and electron energy. Parameters in the expression were obtained from a fit to SPs and IMFPs computed from experimental optical data for a group of 27 elemental solids, and a mean deviation of 10.4 % was found between SPs from optical data and from the new formula. This mean deviation was less than that found in similar comparisons with SPs from empirical modifications of the Bethe SP equation by Joy and Luo and by Fernandez-Varea *et al*. We show illustrative comparisons of SPs calculated from optical data, measured SPs, and SPs from the three predictive SP expressions for C, Si, Cu, Pd, and Pt. The three expressions have been generalized to compounds, and we show similar comparisons for indium antimonide and guanine. The new SP expression is believed to be suitable for Monte Carlo simulations with the continuous slowing-down approximation.

1. Introduction

Monte Carlo (MC) simulation of electron trajectories in solids is a powerful tool in calculations associated with electron-probe microanalysis (EPMA) and surface-sensitive electron spectroscopies such as Auger electron spectroscopy (AES) and X-ray photoelectron spectroscopy (XPS). As indicated in recent reviews [1,2], the trajectories of incident or signal electrons in the sample can be represented as a sum of two independent Poisson stochastic processes describing the elastic and inelastic interactions of the electrons. It is clearly important to use the most reliable available data to describe these interactions. Much effort has been devoted to determine differential cross sections (DCSs) for elastic scattering of electrons by atoms. Twelve sources of elastic DCS data are listed in a recent review [3], and several databases are readily available that provide elastic DCSs in sufficient detail for MC simulations relevant to EPMA, AES, and XPS [4-7]. However, only limited data are available for total cross sections and differential cross sections as a function of energy loss for inelastic scattering of electrons in solids.

Inelastic cross sections are needed in MC simulations for AES for electron energies between 50 eV and 30 keV. Determination of the surface composition requires knowledge of the so-called backscattering factor that accounts for the change of the Auger-signal intensity due to electrons backscattered from a solid [1,8-12]. Information on the lateral distribution of backscattered electrons leads to evaluations of the analysis area and the lateral resolution in scanning Auger microscopy (SAM) [13,14].

The Tougaard "universal" cross sections [15,16] provide approximate descriptions of the differential inelastic-scattering cross sections (or, equivalently, the differential inverse inelastic mean free path (DIIMFP)) in different types of materials for relatively small energy losses (less than about 50 eV). The Tougaard expressions are useful in analyses of XPS spectra for electron energies between about 300 eV and 1500 eV [17]. For MC simulations in AES, we need similar expressions that could be used for a range of materials over a wider range of energy losses and a wider range of electron energies.

Another approach is to assume that the DIIMFP, $K(E,T)$, for electron energy E and energy loss T, is proportional to the electron energy-loss function (ELF) [12],

$$K(E,T) \propto \mathrm{Im}\left[-\frac{1}{\varepsilon(\omega,q)}\right] \qquad (1)$$

where $\varepsilon(\omega,q)$ is the complex dielectric constant, ω is frequency (related to energy loss by $T=\hbar\omega$), and q is the

momentum transfer. Since optical data are available for certain elemental solids and compounds, the DIIMFP can be obtained in the optical limit, i.e., for $q \to 0$. This approach was very effective in calculations of the backscattering factor [12] although there were major computational difficulties in creating the sampler providing the energy losses due to the complex shape of the loss function in some solids. Furthermore, this method is limited to those solids for which the needed loss functions are available.

The difficulties of simulating individual electron energy losses can be overcome with the so-called continuous slowing down approximation (CSDA) that has been frequently used in MC simulations for EPMA. The CSDA is based on the assumption that the electron energy decreases continuously as a function of distance traveled in a solid. The inelastic interactions in a given solid are described by the stopping power (SP), $S = -dE / dx$, a function giving the energy change, dE, per increment of trajectory, dx. Considerable data are available for the stopping power in different materials [7,18,19]. In addition, a number of analytical expressions [20-22], based in general on the nonrelativistic Bethe SP equation [23], have been proposed for the SP in any material. Unfortunately, the Bethe expression is not valid for electron energies smaller than about 10 keV [24] and consequently should not be used in simulations of electron transport for AES and XPS applications. Modifications to the Bethe formula have been made to extend its range of utility [20-22] but this approach is limited to the particular solids for which needed parameters have been determined [25].

There is an obvious need for a universal source of SPs for electron energies below 10 keV. We have recently proposed [25] an empirical predictive expression for the SP based on SPs and inelastic mean free paths (IMFPs) calculated from optical data for a group of 27 elemental solids [24,26]. This expression was considered useful for electron energies between 200 eV and 30 keV. In the following sections, we present a short review of these results (with data for C, Si, Cu, Pd, and Pt) and show comparisons of SPs calculated from optical data for two compounds (indium antimonide and guanine) with SPs from our predictive expression and two others [21,22].

2. Calculations of the stopping power and the inelastic mean free path

Penn [27] has described an algorithm for the calculation of electron IMFPs from a model dielectric function $\varepsilon(\omega,q)$. The differential inelastic-scattering cross section, per atom or molecule, for an electron in an infinite medium is:

$$\frac{d^2\sigma}{dq d\omega} = \frac{m e_0^2}{\pi M \hbar E} \mathrm{Im}\left(\frac{-1}{\varepsilon(\omega,q)}\right)\frac{1}{q} \qquad (2)$$

where m is the electronic mass, e_0 is the electronic charge, and M is the density of atoms or molecules per unit volume. The dependence of the ELF on ω can be obtained from experimental optical data for the material of interest (for $q = 0$) and the dependence of the ELF on q can be obtained from an appropriate theoretical model [28]. In our work, we utilized the Lindhard [29] dielectric function to describe the q-dependence of the ELF. The IMFP can be obtained from an integration of Eq. (2) over the kinematically allowed regions of ω and q [30]. The SP can be obtained from a similar integration of the ELF multiplied by (ω/q) [18,24].

3. Predictive formulas for the stopping power

3.1 The S-lambda approach

The differential inelastic-scattering cross section, $d\sigma_{in} / dT$, is related to the DIIMFP by:

$$K(E,T) = \frac{d\lambda_{in}^{-1}}{dT} = M \frac{d\sigma_{in}}{dT} \qquad (3)$$

where λ_{in} is the IMFP and M is the atomic density. The stopping power can be defined from the above equation as:

$$S = \int M\ T \frac{d\sigma_{in}}{dT}\, dT = \int T\ K(E,T)\, dT \qquad (4)$$

where the integration is extended over the allowed range of energy losses. On the other hand, the IMFP is expressed by the DIIMFP according to the obvious relation:

$$\lambda_{in} = \left(\int_0^E K(E,T)\, dT\right)^{-1} \qquad (5)$$

Assuming that the allowed range of energy losses extends up to the current energy E, Eqs. (4) and (5) lead to the expression [1,31]:

$$S\lambda_{in} = \frac{\int_0^E T\ K(E,T)\, dT}{\int_0^E K(E,T)\, dT} = \langle T \rangle \qquad (6)$$

where $\langle T \rangle$ is the mean energy loss for an inelastic interaction. As follows from Eq. (6), the mean energy loss must be a monotonically increasing function of E since the DIIMFP is always positive. We observe a maximum in the loss function [and in the DIIMFP, as follows from Eq. (1)] usually below 100 eV. Thus, we may expect that the mean energy loss, $\langle T \rangle = S\lambda_{in}$, is a relatively weak function of energy at energies exceeding 100 eV.

IMFPs and SPs were calculated from experimental optical data for 27 elemental solids (C, Mg, Al, Si, Ti, V, Cr, Fe, Ni, Cu, Y, Zr, Nb, Mo, Ru, Rh, Pd, Ag, Hf, Ta, W, Re, Os, Ir, Pt, Au, and Bi) [24,26]. For each element, IMFPs and SPs were calculated for 81 energies that were equally spaced on a logarithmic scale between 10 eV and 30 keV. Analysis of the products $S\lambda_{in}$ led to the following SP predictive formula [25]:

$$S_{SL}(Z,E) = \frac{c_1(c_2 Z + 1)\ln(c_3 E)}{\lambda_{in}} \quad \text{(eV/Å)} \qquad (7)$$

where Z is the atomic number, E is expressed in eV, λ_{in} is expressed in Å, and c_1, c_2, and c_3 are fitted coefficients. From a fit to the combined data set for energies between 200 eV and 30 keV, the following values of the coefficients were obtained: $c_1 = 11.52$, $c_2 = 0.01639$, and $c_3 = 0.03386$. The mean percentage deviation, ΔS_j, between SPs calculated from optical data, S_{ij}, and SPs predicted from Eq. (7) for the ith energy and the jth element (with atomic number Z_j) can be obtained from:

$$\Delta S_j = 100\,\frac{1}{n_E}\sum_{i=1}^{n_E}\frac{\left|S_{ij} - S_{SL}(Z_j, E_i)\right|}{S_i} \qquad (8)$$

where n_E is the number of energies. Values of ΔS_j for the 27 considered elements are shown in Fig. 1 (the data point for C is for glassy carbon). The mean percentage deviation averaged additionally over all elements was found to be 10.4 %.

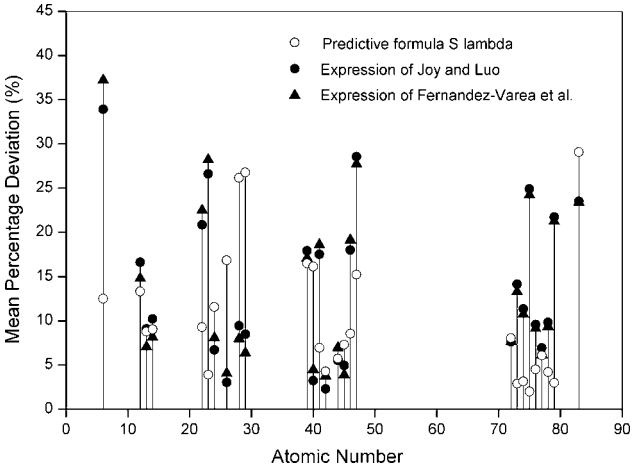

Fig. 1. Mean percentage deviations between stopping powers calculated from optical data and values from three analytical SP expressions for 27 elemental solids. Open circles: the S-lambda expression [Eq. (7)]; filled circles: the expression of Joy and Luo [Eq. (10)]; filled triangles: the expression of Fernandez-Varea *et al.* [Eq. (11)].

3.2 Modified Bethe equation

A universal expression for the SP was derived by Bethe in the 1930s [23]. This expression relates the SP to the current electron energy in an elemental solid,

$$S = -\frac{dE}{dx} = 2\pi e_0^4 N_0 \frac{Z\rho}{AE}\ln\left(\frac{\sqrt{(e/2)}\,E}{J}\right) \qquad (9)$$

where e = 2.718 is the base for natural logarithms, N_0 is the Avogadro constant, ρ is the density, A is the atomic mass, E is the current energy, and J is the mean excitation energy. The Bethe equation is known to fail at low electron energies. For $E < J/1.166$(e.g., E < 67 eV for C and E < 678 eV for Pt [18]), the stopping power becomes negative which is physically unrealistic. The Bethe equation is also unlikely to be valid for energies less than about 10 keV [24].

Several attempts have been made to modify the Bethe equation to extend its validity to lower energies [20-22]. We consider here two modifications [21,22] to the Bethe equation that have been used to fit SPs calculated from optical data for the group of 27 elemental solids indicated above [25].

1. Equation of Joy and Luo [21]. This equation can be transformed to the following general form:

$$S_{JL}(Z,E) = 785\frac{Z\rho}{AE}\ln\left(\frac{1.166E}{d_1 Z} + d_2\right) \quad \text{(eV/Å)} \qquad (10)$$

where ρ is in g/cm^3 and E is in eV. The minimization procedure, performed in the energy range from 200 eV to 30 keV, leads to the following values for the coefficients: $d_1 = 12.35$, and $d_2 = 1.174$. The mean percentage deviations between values of $S_{JL}(Z,E)$ from Eq. (10) and the calculated SPs (found by a procedure analogous to Eq. (8)) are shown in Fig. 1. The mean percentage deviation averaged over the 27 elements was found to be 13.8 %.

2. Equation of Fernandez-Varea *et al.* [22]. Their equation can be generalized to the form:

$$S_{FV}(Z,E) = 785\frac{Z\rho}{AE}\left[\ln\left(\frac{1.166E}{e_1 Z}\right) + e_2\left(Z\frac{R}{E}\right) + e_3\left(Z\frac{R}{E}\right)^2\right] \quad \text{(eV/Å)} \qquad (11)$$

where R = 13.6 eV is the Rydberg energy. The fit of Eq. (11) to the calculated SPs over the same energy range gave the following values of the coefficients: $e_1 = 13.74$, $e_2 = 0.5530$, and $e_3 = -0.04782$. The mean percentage deviations between values of $S_{FV}(Z,E)$ from Eq. (11) and the calculated SPs by a similar procedure are shown in Fig. 1. The mean percentage deviation for all considered elements and energies was 13.7 %.

We see that that the mean percentage deviation for all 27 elemental solids between SPs from the S-lambda approach and SPs calculated from optical data leads (10.4 %) is less than the corresponding values for the Joy and Luo and Fernandez-Varea *et al.* expressions (13.8 % and 13.7 %, respectively). In addition, Fig. 1 indicates that mean percentage deviation for each solid from the S-lambda approach is often lower than the corresponding values for the other two approaches although these deviations are larger than the other approaches for Cr, Fe, Ni, Cu, Hf, and Bi.

4. Compounds

The predictive SP formula [Eq. (7)] was derived from an extensive database of SPs calculated for 27 elemental solids. In practice, SPs are also needed for multicomponent solids, i.e., alloys and compounds. We therefore need to test whether the predictive SP formulas described above are applicable to any solid.

We first rewrite the Bethe SP equation [Eq. (9)] for an elemental solid:

$$S = 2\pi\, e_0^4\, \frac{M\, Z}{E} \ln\left(\frac{\sqrt{(e/2)}\, E}{J}\right) \tag{12}$$

The SP for a multicomponent solid can be approximated by the weighted sum of the stopping powers of the atomic constituents of the solid with weights given by the mass fractions [18,32]. Equation (10) can then be generalized in the following way for a multicomponent solid:

$$\begin{aligned} S &= 2\pi\, e_0^4 \sum_{k=1}^{n} \frac{M_k\, Z_k}{E} \ln\left(\frac{\sqrt{(e/2)}\, E}{J_k}\right) \\ &= 2\pi\, e_0^4 \sum_{k=1}^{n} X_k \frac{M\, Z_k}{E} \ln\left(\frac{\sqrt{(e/2)}\, E}{J_k}\right) \end{aligned} \tag{13}$$

where M_k is the atomic density of the *k*th element in the solid, M is now the total atomic density of the solid, Z_k is the atomic number of the *k*th element, X_k is the atomic fraction of the *k*th element, and J_k is the mean excitation energy for the *k*th element. The summation in Eq. (13) is extended over all *n* elements constituting the solid. We have further

$$MX_k = \frac{N_0 \rho}{A_k} C_k \tag{14}$$

where A_k is the atomic mass of the *k*th element, C_k is the mass fraction for the *k*th element, and ρ is now the density of the solid. From Eqs. (13) and (14), we eventually obtain:

$$\begin{aligned} S &= 2\pi\, e_0^4 N_0 \sum_{k=1}^{n} C_k \frac{Z_k \rho}{A_k\, E} \ln\left(\frac{\sqrt{(e/2)}\, E}{J_k}\right) \\ &= 785 \sum_{k=1}^{n} C_k \frac{Z_k \rho}{A_k\, E} \ln\left(\frac{1.166\, E}{J_k}\right) \end{aligned} \quad \text{(eV/Å)} \tag{15}$$

The atomic fractions, X_i, can be obtained from the stoichiometry coefficients for the solid and the mass fractions, C_k, from:

$$C_k = \frac{X_k A_k}{\sum_{j=1}^{n} X_j A_j} \tag{16}$$

Following this procedure, we can now generalize Eqs. (10) and (11) for a multicomponent solid as follows:

$$S_{JL} = 785 \sum_{k=1}^{n} C_k \frac{Z_k \rho}{A_k\, E} \ln\left(\frac{1.166\, E}{d_1 Z_k} + d_2\right) \quad \text{(eV/Å)} \tag{17}$$

and

$$S_{FV} = 785 \sum_{k=1}^{n} C_k \frac{Z_k \rho}{A_k\, E} \ln\left[\frac{1.166\, E}{e_1 Z_k} + e_2\left(Z_k \frac{R}{E}\right) + e_3\left(Z_k \frac{R}{E}\right)^2\right] \quad \text{(eV/Å)} \tag{18}$$

The predictive SP formula obtained for elemental solids from the S-lambda approach is an explicit function of the atomic number and energy [Eq. (7)]. The dependence on the atomic weight and density is indirect via the IMFP. We therefore generalize Eq. (7) to a multicomponent solid:

$$\begin{aligned} S_{SL} &= \sum_{k=1}^{n} C_k \frac{c_1 (c_2 Z_k + 1) \ln(c_3 E)}{\lambda_{in}} \\ &= \frac{1}{\lambda_{in}} c_1 \ln(c_3 E)\left(1 + c_2 \sum_{k=1}^{n} C_k Z_k\right) \end{aligned} \quad \text{(eV/Å)} \tag{19}$$

The IMFP for a multicomponent solid can be calculated from the TPP-2M formula [33]:

$$\lambda_{in} = \frac{E}{E_p^2[\beta \ln(\gamma E) - (C/E) + (D/E^2)]} \quad \text{(in Å)} \tag{20}$$

$$\beta = -0.10 + 0.944(E_p^2 + E_g^2)^{-1/2} + 0.069\rho^{0.1}$$

$$\gamma = 0.191\rho^{-1/2}$$

$$C = 1.97 - 0.91U$$

$$D = 53.4 - 20.8U$$

$$U = N_v \rho / A = E_p^2 / 829.4$$

where $E_p = 28.8(N_v \rho / A)^{1/2}$ is the free-electron plasmon energy (in eV), N_v is the number of valence electrons per atom (for elemental solids) or molecule (for compounds), A denotes here the atomic or molecular weight, and E_g is the bandgap energy (in eV).

5. Results and discussion

Figures 2–6 show comparisons of SPs calculated from optical data for five illustrative elemental solids [24,26] with measured SPs [7,34-37] and with SPs obtained from the three generalized SP formulas described here. The selected solids (C, Si, Cu, Pd, and Pt) cover a wide range of atomic numbers. Most of the measured SPs were taken from Joy's SP database [7]. Although calculated SPs are shown in Figs. 2-8 for energies between 10 eV and 100 eV, these values are not as reliable as those for higher energies [24] and are included here to show general trends as a function of energy.

The upper panels of Figs. 2–6 show reasonably good agreement between SPs calculated from optical data and the measured SPs. Note that the experimental SPs for carbon shown in Fig. 2(a) were measured for graphite and agree well

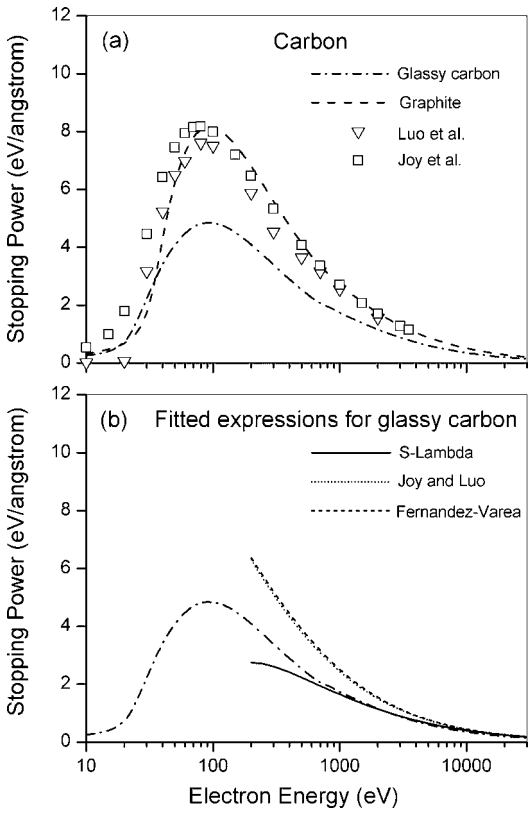

Fig. 2. Comparison of stopping powers calculated from optical data by Tanuma *et al*. [26] for glassy carbon (dot-dashed line) and graphite (long-dashed line) with (a) measured SPs for graphite (symbols) and (b) SPs computed for glassy carbon from the S-lambda approach, Eq. (7) (solid line), the Joy and Luo expression, Eq. (10) (dotted line), and the Fernandez-Varea *et al.* expression, Eq. (11) (dashed line). Inverted triangles: SPs from Luo *et al.* [7,34]; squares: Joy *et al.* [7,35].

with the corresponding calculated SPs. We also show calculated SPs for glassy carbon in Figs. 2(a) and (b) since these SPs were part of our initial evaluation of the S-lambda approach [25] in which we compared the calculated SPs with values from the three predictive expressions. Figure 2(b) shows that SPs from the S-lambda approach agree much better with the computed SPs than values from Eqs. (17) and (18) (as shown in Fig. 1). Furthermore, there is some difference between two sets of measured SPs for platinum from the same group [34,35] but there is better agreement between the later (and presumably more reliable) measurements [35] with the SPs calculated from optical data [24].

We now show similar comparisons in Figs. 7 and 8 for two compounds, one inorganic compound (InSb) and one organic compound (guanine). For InSb, we have $X_{In} = X_{Sb} = 0.5$. We obtain the following mass fractions from Eq. (16): $C_{In} = 0.4853$ and $C_{Sb} = 0.5147$. These values are used in calculations of SPs from the three predictive expressions [Eqs. (17), (18), and (19)]. The IMFP values needed for Eq. (19) were calculated from experimental optical data [38]. As shown in Fig. 7(a), there is a distinct difference in the shapes of the calculated and measured SPs. For energies exceeding 200 eV, however, there is reasonable agreement. Figure 7(b) indicates that SPs from the S-lambda predictive formula and from the Joy and Luo expression compare well with the calculated SPs. SPs from the expression of Fernandez-Varea *et al*. appreciably underestimate the calculated SPs for $E < 1$ keV.

For guanine ($C_5H_5ON_5$), the atomic fractions are: $X_C = X_H = X_N = 0.3125$, and $X_O = 0.0625$. The mass fractions calculated from Eq. (16) are: $C_C = 0.3974$, $C_H = 0.0333$, $C_O = 0.1059$, and $C_N = 0.4634$. There is very good agreement between the measured and calculated SPs for guanine in Fig. 8(a). SPs from the S-lambda approach underestimate SPs calculated from optical data for $E < 1$ keV in Fig. 8(b) while SPs from the generalized Joy and Luo and Fernandez-Varea *et al*. expressions both agree well with the calculated SPs.

6. Summary

We have developed an analytical expression for the product of the SP and IMFP, the S-lambda expression [Eq. (7)]. This expression, an empirical function of Z and E, empirically describes SPs computed from optical data for a group of 27 elemental solids [24] with a mean relative deviation of about 10 % for electron energies between 200 eV and 30 keV. This expression is superior to two alternative SP predictive expressions based on modifications of the Bethe stopping-power equation by Joy and Luo [21] and by Fernandez-Varea *et al*. [22]. Illustrative comparisons are shown for C, Si, Cu, Pd, and Pt.

We also show comparisons of SPs from a generalized form of the S-lambda expression [Eq. (19)] with SPs calculated from optical data for two compounds, indium antimonide and guanine [26]. SPs from the generalized S-lambda expression agreed well with the calculated SPs for InSb but there was poorer agreement for guanine for $E < 1$ keV. SPs from generalized forms of the Joy and Luo and Fernandez-Varea *et al.* expressions [Eqs. (17) and (16)] agreed well with the computed SPs for guanine but, for InSb, there was agreement only with SPs from the Joy and Luo expression.

The new S-lambda expression is believed to be suitable for Monte Carlo simulations with the continuous slowing-down approximation for energies between 200 eV and 30 keV.

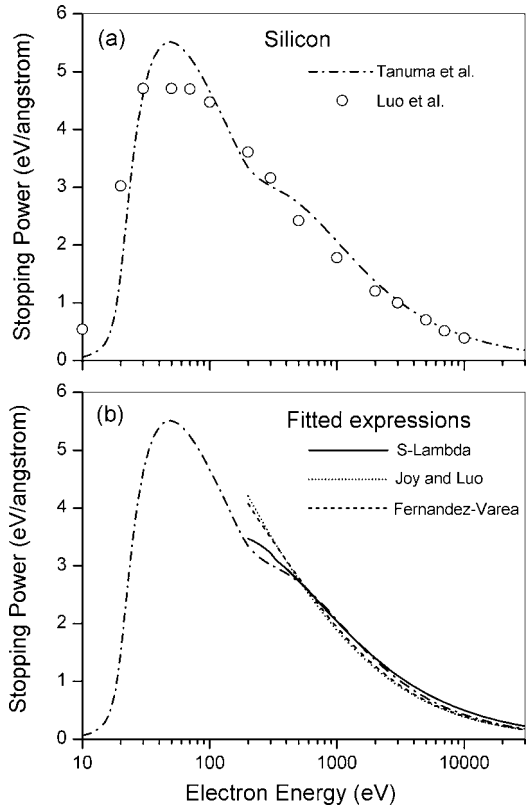

Fig. 3 Comparison of stopping powers calculated from optical data by Tanuma *et al*. [24] (dot-dashed line) for silicon with (a) measured SPs (symbols) and (b) SPs computed from the S-lambda approach, Eq. (7) (solid line), the Joy and Luo expression, Eq. (10) (dotted line), and the Fernandez-Varea *et al.* expression, Eq. (11) (dashed line). Circles: SPs from Luo *et al.* [7,36].

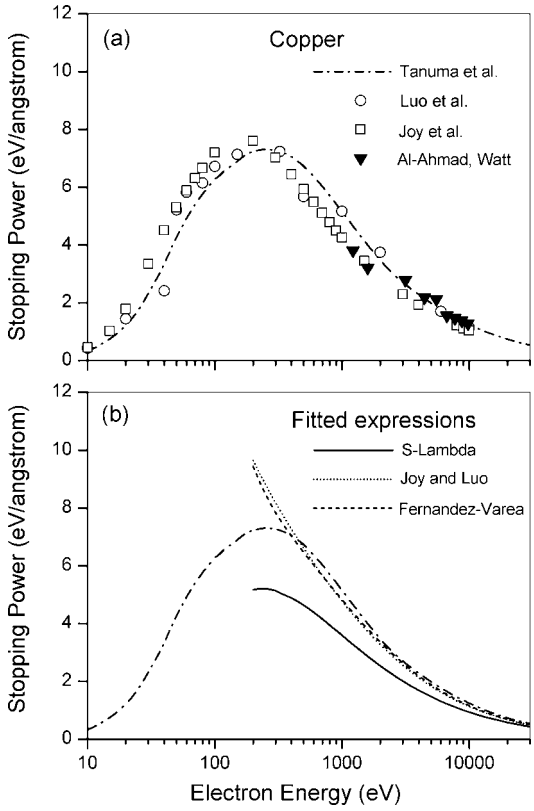

Fig. 4 Same as Fig. 3 except for copper. Circles: Luo *et al*. [7,36]; inverted triangles: Joy *et al.* [7,35]; squares: Al-Ahmad and Watt [37].

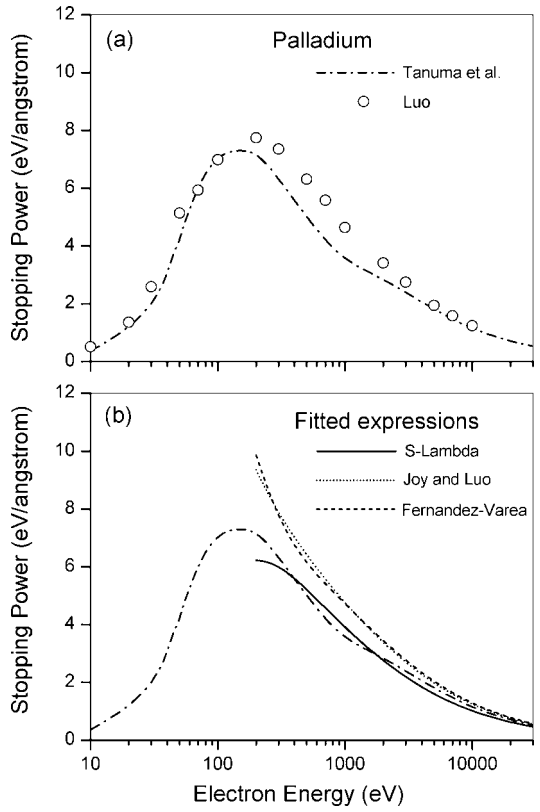

Fig. 5 Same as Fig. 3 except for palladium. Circles: Luo [7,34].

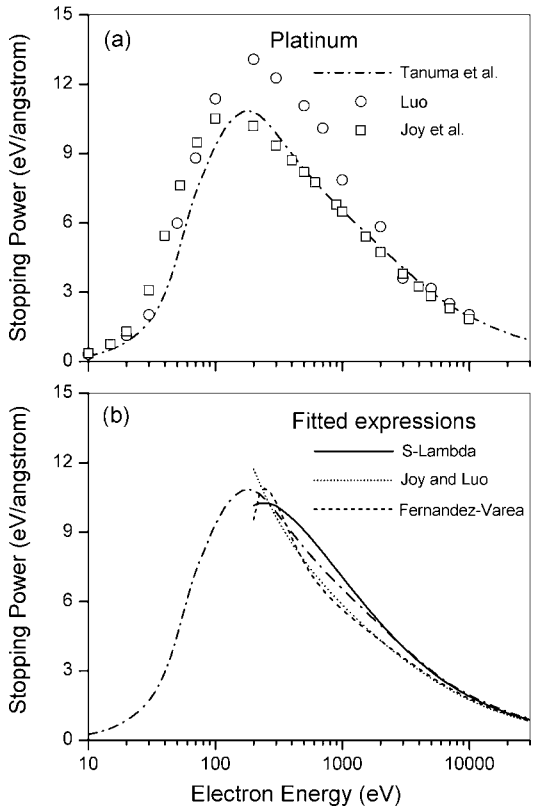

Fig. 6 Same as Fig. 3 except for platinum. Circles: Luo [7,34]; squares: Joy *et al.* [7,35].

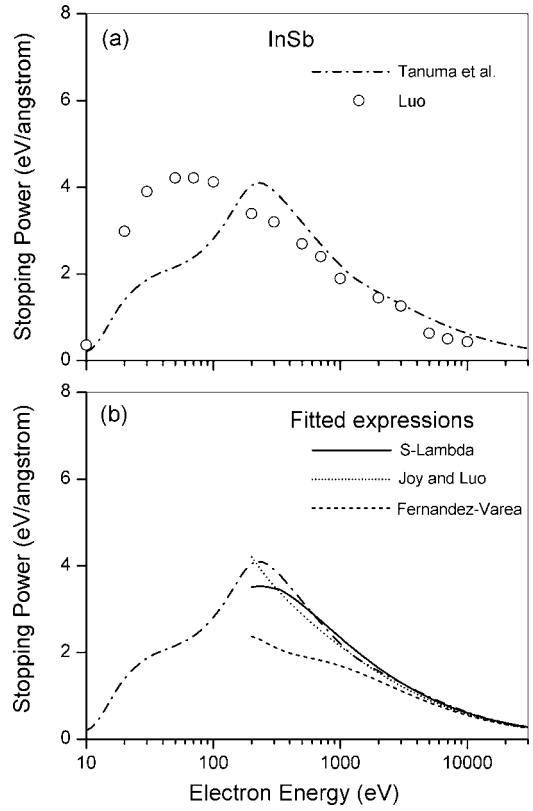

Fig. 7 Comparison of stopping powers calculated from optical data by Tanuma *et al*. [26] (dot-dashed line) for indium antimonide with (a) measured SPs (symbols) and (b) SPs computed from the generalized S-lambda (Eq. (19), solid line), Joy and Luo (Eq. (17), dotted line), and Fernandez-Varea *et al.* (Eq. (18), dashed line) approaches. Circles: Luo .[7,34].

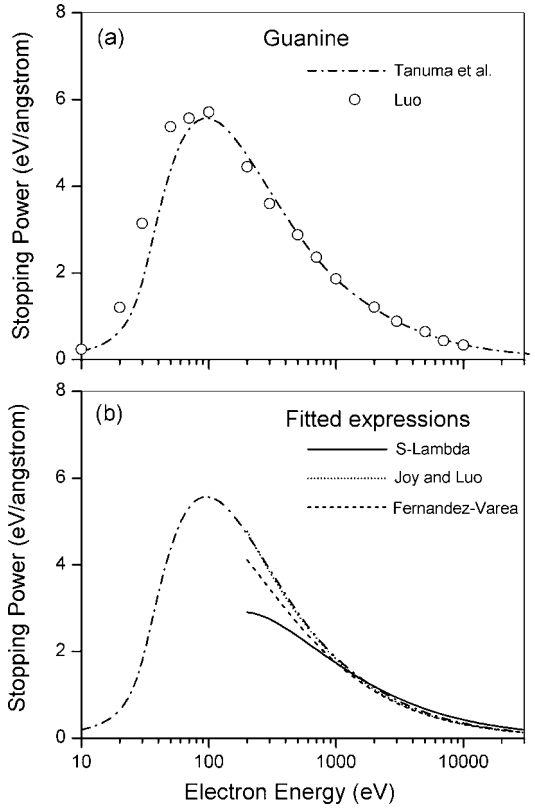

Fig. 8 Same as Fig. 7 except for guanine. Circles: Luo .[7,34].

Acknowledgment

One of the authors (A. J.) would like to acknowledge partial support by the Foundation for Polish Science. Another author (S. T.) acknowledges the New Energy and Industrial Technology Development Organization for its financial support.

References

[1] A. Jablonski, C. J. Powell, and S. Tanuma, *Surf. Interface Anal*. **37**, 861 (2005)
[2] A. Jablonski, Prog. *Surf. Sci.* **79**, 3 (2005).
[3] A. Jablonski, F. Salvat, and C. J. Powell, *J. Phys. Chem. Ref. Data* **33**, 409 (2004).
[4] F. Salvat, A. Jablonski, and C. J. Powell, *Comput. Phys. Commun.* **165**, 157 (2005).
[5] A. Jablonski, F. Salvat, and C. J. Powell, *NIST Electron Elastic-Scattering Cross-Section Database* , Version 3.1, *Standard Reference Data Program Database* 64, U.S. Department of Commerce, National Institute of Standards and Technology, Gaithersburg, MD, 2003; web address: http://www.nist.gov/srd/nist64.htm.
[6] Z. Czyzewski, D. O. MacCallum, A. Romig, and D. C. Joy, *J. Appl. Phys.* **68**, 3066 (1990).
[7] D. C. Joy, *A Database of Electron-Solid Interactions*, Metrology and Lithography Group of the University of Tennessee, 2004, web address: http://pciserver.bio.utk.edu/metrology.
[8] R. Shimizu and S. Ichimura, *Quantitative Analysis by Auger Electron Spectroscopy*, Toyota Foundation Research Report No. I-006 76-0175, Tokyo, 1981.
[9] S. Ichimura and R. Shimizu, *Surf. Sci.* **112**, 386 (1981).
[10] S. Ichimura, R. Shimizu, and J. P. Langeron, *Surf. Sci*. **124,** L49 (1983).
[11] R. Shimizu, *Japanese J. Appl. Phys*. **22,** 1631 (1983).
[12] A. Jablonski and C. J. Powell, *Surf. Sci*. **574**, 219 (2005).
[13] C. J. Powell, Appl. *Surf. Sci.* **230**, 327 (2004).
[14] A. Jablonski and C. J. Powell, *Appl. Surf. Sci*. **242**, 220 (2005).
[15] S. Tougaard, *Solid State Comm*. **61**, 547 (1987).
[16] S. Tougaard, *Surf. Interface Anal*. **25**, 137. (1997).
[17] S. Tougaard, *Surf. Interface Anal*. **26**, 249 (1999).
[18] *Stopping Powers for Electrons and Positrons*, ICRU Report 37. International Commission on Radiation Units and Measurements, Bethesda, MD, 1984.
[19] M. J. Berger, J. S. Coursey, and M. A. Zucker, *Stopping-Power and Range Tables for Electrons, Positrons and Helium Ions.* Web address: http://physics.nist.gov/PhysRefData/Star/Text/contents.html.
[20] T. S. Rao-Sahib and D. B. Wittry, *J. Appl. Phys.* **45**, 5060 (1974)
[21] D. C. Joy and S. Luo, *Scanning* **11**, 176 (1989).
[22] J. M. Fernandez-Varea, R. Mayol, D. Liljequist, and F.

Salvat, *J. Phys. Cond. Matter* **5**, 3593 (1993).
[23] H. Bethe, Ann. Phys. Leipzig, **5**, 325 (1930); H. Bethe, in: *Handbook of Physics*, Vol. 24, Springer, Berlin, 1933, p.273.
[24] S. Tanuma, C. J. Powell, and D. R. Penn, *Surf. Interface Anal*. **37**, 978 (2005).
[25] A. Jablonski, S. Tanuma, and C. J. Powell, *Surf. Interface Anal*. **38**, 76 (2006).
[26] S. Tanuma, C. J. Powell and D. R. Penn (to be published).
[27] D. R. Penn, *Phys. Rev*. B **35**, 482 (1987).
[28] C. J. Powell and A. Jablonski, *J. Phys. Chem. Ref. Data* **28**, 19 (1999).
[29] J. Lindhard, *Kgl. Danske Videnskab. Selskab. Mat.-Fys. Medd*. **28** (no. 8), 1 (1954); J. Lindhard and M. Scharff, *Kgl. Danske Videnskab. Selskab. Mat.-Fys. Medd.* **27** (no. 15), 1 (1953); J. Lindhard, M. Scharff and H. E. Schiott, *Kgl. Deanske Videnskab. Selskab. Mat.-Fys. Medd.* **33** (no. 14), 1 (1963).
[30] S. Tanuma, C. J. Powell and D. R. Penn, *Surf. Interface Anal*. **17**, 911 (1991).
[31] J. M. Fernandez-Varea, F. Salvat, M. Dingfelder and D. Liljequist, *Nucl. Instr. Methods Phys. Res.* B **229**, 187 (2005).
[32] S. J. B. Reed, *Electron Probe Microanalysis*, second edition (Cambridge University Press, 1993), pp. 193-194.
[33] S. Tanuma, C. J. Powell and D. R. Penn, *Surf. Interface Anal*. **21**, 165 (1994).
[34] S. Luo, *Study of Electron-Solid Interactions*, Ph.D. Thesis, University of Tennessee (1994).
[35] D. C. Joy, S. Luo, R. Gauvin, P. Hovington and N. Evans, *Scanning Microscopy* **10**, 653 (1996).
[36] S. Luo, X. Zhang and D. C. Joy, *Rad. Eff. Defects Solids* **117**, 235 (1991).
[37] K. O. Al-Ahmad and D. E. Watt, *J. Phys. D, Appl. Phys.* **16**, 2257 (1983).
[38] S. Tanuma, C. J. Powell and D. R. Penn (to be published).